AIP Journal of Applied Physics

Temperature dependence of the electronic transitions in BiFeO3 thin film studied by spectroscopic ellipsometry

T. D. Kang, B. C. Jeon, and S. J. Moon

Citation: Journal of Applied Physics **117**, 134107 (2015); doi: 10.1063/1.4916722
View online: http://dx.doi.org/10.1063/1.4916722
View Table of Contents: http://scitation.aip.org/content/aip/journal/jap/117/13?ver=pdfcov
Published by the AIP Publishing

Temperature dependence of the electronic transitions in $BiFeO_3$ thin film studied by spectroscopic ellipsometry

T. D. Kang,[1,2] B. C. Jeon,[1,2] and S. J. Moon[3,a)]
[1]*Center for Correlated Electron Systems, Institute for Basic Science, Seoul 151-742, South Korea*
[2]*Department of Physics and Astronomy, Seoul National University, Seoul 151-742, South Korea*
[3]*Department of Physics, Hanyang University, Seoul 133-791, South Korea*

(Received 22 December 2014; accepted 21 March 2015; published online 6 April 2015)

The temperature dependence of the electronic response of $BiFeO_3$ thin film grown on a $SrTiO_3$ substrate is investigated using spectroscopic ellipsometry. By analyzing the pseudodielectric function, we identify two *d-d* crystal field transitions of Fe^{3+} ions in the energy region between 1 and 2 eV. The *d-d* transitions show abnormal temperature dependence that cannot be attributed to conventional electron-phonon interactions. The origin of the abnormal temperature dependence is discussed in terms of spin-charge coupling. The temperature dependence of the charge transfer transitions located above 2.5 eV is characterized by standard critical point model analysis of the 2nd derivatives of the dielectric function. This analysis provides detailed information of the critical point parameters for charge transfer transitions. © *2015 AIP Publishing LLC*.
[http://dx.doi.org/10.1063/1.4916722]

I. INTRODUCTION

Bismuth ferrite ($BiFeO_3$, abbreviated as BFO) has attracted a great deal of interest due to its unique room-temperature ferroelectric and canted antiferromagnetic order properties. The ferroelectric and antiferromagnetic transition temperatures of bulk BFO crystals are about 1103 K and 643 K, respectively.[1,2] Multiferroic BFO also exhibits magnetoelectric effects, indicating close coupling between charge and spin.[3]

The effects of spin-charge coupling in BFO single crystals have been demonstrated in recent optical studies.[4,5] Ramirez *et al*. observed the magnon sidebands in second harmonic generation data at room temperature.[4] Magnon sidebands can appear when electric dipole active magnetic excitations couple to electronic excitations. The relevant electronic excitations in BFO were on-site *d-d* crystal field (CF) excitations of Fe^{3+} ions located below its fundamental band gap.[5,6] The intensity of the magnon sidebands in the second harmonic generation data increased markedly below the antiferromagnetic transition temperature, T_N, suggesting coupling between the *d-d* CF transitions and the Fe^{3+} spin states of Fe^{3+}.[4] Xu *et al*. performed linear absorption spectroscopy and found an anomaly in the temperature (T) dependence of the CF transition of Fe^{3+} ions; the oscillator strength of the magnon sideband peaks showed a minimum at about 140 K.[5] We note that Raman experiments on BFO found an anomaly at this T.[7,8] Furthermore, they observed the magnon sidebands associated with *d-d* crystal field excitations of Fe^{3+} ions at low T under a magnetic field.[5]

Raman studies of BFO suggested that this anomaly in the optical data were associated with spin-reorientation transitions.[7,8] Cazayous *et al*. reported that the magnon excitations in Raman spectra of BFO single crystals showed anomalies in their intensity and peak positions at $T = 140$ K: the intensity of the magnon peaks exhibited a maximum, and the energy value of the magnon peak decreased slightly.[7] Singh *et al*. observed similar anomalies in magnon excitations in Raman spectra of BFO at $T = 140$ and 200 K.[8] They suggested that these anomalies in Raman spectra may indicate a spin reorientation transition similar to those observed in most rare earth orthoferrites.[8–10]

To our knowledge, the effects of spin-charge coupling manifested in the optical response from *d-d* CF excitations have not been reported for BFO films. Although there have been some T-dependent optical studies on BFO thin films, they focused on the *p-d* charge transfer transitions.[11,12] We note that for epitaxial BFO films, room temperature spontaneous polarization and magnetization are enhanced compared to BFO single crystals. Therefore, stronger spin-charge coupling may be expected in BFO films. In addition, lattice deformation in thin films due to substrate strain may also affect spin-charge coupling. In multiferroic materials, the lattice is coupled to spin through magnetoelastic or magnetostriction interactions.[13–15] These thin film characteristics may lead to anomalies in the *d-d* CF excitations in BFO films that differ from those of single crystals.

In this study, we investigate T dependence of the electronic transitions of rhombohedral BFO thin film grown epitaxially on (001) $SrTiO_3$ (STO) substrate using spectroscopic ellipsometry. We identified two *d-d* CF transitions below 2 eV and five charge transfer transitions between 2 and 5 eV. We observed that the *d-d* CF transitions exhibited an anomaly at about 200 K, at which a Raman study found the signature of a spin-reorientation transition.[8] The charge transfer transitions are analyzed using the standard critical model. The analysis provided detailed information on the critical point parameters for charge transfer transitions. The signature of spin-charge coupling was observed in the T dependence of the critical point parameters.

a)soonjmoon@hanyang.ac.kr

II. EXPERIMENTS

BFO thin film deposited on a STO (001) substrate was prepared using pulsed laser deposition (PLD) with an oxygen partial pressure of 300 mTorr and maintaining substrate T at 570 °C. The power and frequency of the laser were 2.8 J/cm^2 and 5 Hz, respectively. The crystalline quality and phase of the BFO film were identified by X-ray diffraction measurement (Bruker D8 Discover), and the roughness of the film surface was estimated using atomic force microscopy (AFM). Ellipsometric angles (Ψ and Δ) were measured with temperature dependence at an incidence angle of 70° in the energy region between 0.74 and 5.5 eV using a spectroscopic ellipsometer (VASE model; J.A. Woollam Co.). Ellipsometric measurement is a powerful tool for investigating the optical response of thin films as it is performed at oblique incidence angles and measures both the intensity and phase of light.[16,17]

III. RESULTS AND DISCUSSIONS

Figure 1 shows the X-ray diffraction pattern for the BFO film on STO substrate (BFO/STO) with θ–2θ configuration. Diffraction peaks from the (001) and the (002) planes of the BFO were observed around 22° and 45°, respectively, confirming dominance of the rhombohedral crystalline phase.[18] The root mean square surface roughness, estimated by AFM measurement, was around 2.5 nm.

Figure 2(a) shows the raw pseudodielectric functions $\langle\varepsilon\rangle$ of BFO/STO for $T = 80$ and 400 K. The pseudodielectric function was converted from the ellipsometric angles using the following equation:

$$\langle\varepsilon\rangle = \sin^2\theta_i\left[1 + \tan^2\theta_i\left(\frac{1-\rho}{1+\rho}\right)^2\right], \quad (1)$$

where θ_i is the incident angle of light and $\rho = \tan\Psi\exp(i\Delta)$.[19]

The dielectric function of the BFO thin film can be obtained by fitting the pseudodielectric function. The sample was assumed to be composed of three layers, i.e., STO substrate, BFO thin film, and surface roughness layer. The best fit for the pseudodielectric function of the BFO film was achieved using a Kramers-Konig consistent multiple Gaussian oscillator model.[20] The optical constants of STO substrate obtained from the ellipsometry measurement at each measurement temperature were used for the layer model analysis. The fitting results are plotted with solid lines in Fig. 2(a). The thicknesses of the BFO film and the surface roughness layer were estimated to be about 69 nm and 2.2 nm, respectively. Note that the thickness of the surface roughness layer estimated from the ellipsometric analysis was consistent with the AFM result.

The 2nd derivative of the optical function with respect to photon energy enhances structures in the spectra, thus enabling more accurate lineshape analysis.[21] Therefore, analysis of the 2nd derivative of the pseudodielectric function can

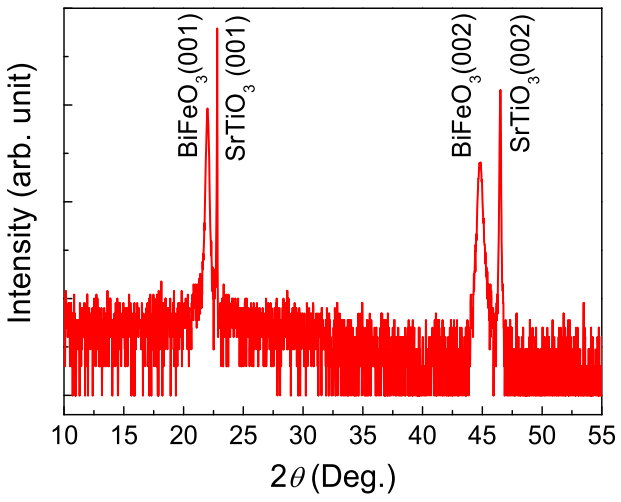

FIG. 1. (a) X-ray diffraction data of $BiFeO_3$ thin film on $SrTiO_3$ substrate measured with θ–2θ configuration.

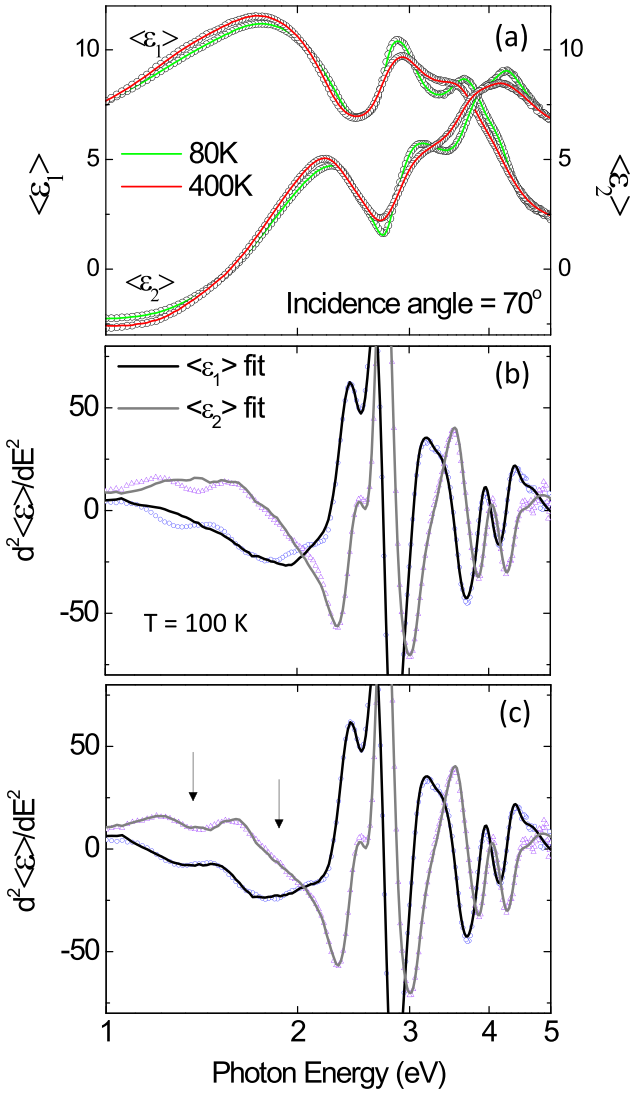

FIG. 2. (a) Raw pseudodielectric function ($\langle\varepsilon_1\rangle + i\langle\varepsilon_2\rangle$) data at $T = 80$ K and 400 K. Symbol: experimental data. Solid line: fitting result using multiple Gaussian oscillator model. (b) The 2nd derivatives of the pseudodielectric function at $T = 100$ K (symbol). Solid lines are the 2nd derivatives of the fitting result of pseudodielectric function at $T = 100$ K. (c) The 2nd derivatives of the pseudodielectric function at $T = 100$ K (symbol). Solid lines are the 2nd derivatives of the fitting result of the pseudodielectric function after inclusion of two oscillators for d-d transitions.

help to identify weak optical transitions such as *d-d* CF transitions. Indeed, the 2nd derivatives of the pseudodielectric function clearly reveal some distinctive transitions in the energy region between 1 and 2 eV, which are not captured in analysis of the raw pseudodielectric function. Figure 2(b) highlights the sensitivity of the 2nd derivatives of the pseudodielectric function for detecting weak features in the optical response. The solid lines in Fig. 2(b) are from the fitting results of the raw $\langle\varepsilon\rangle$ (Fig. 2(a)). It can be seen that the 2nd derivatives of the $\langle\varepsilon\rangle$ are clearly different from those of the fitting results of $\langle\varepsilon\rangle$ below 2.2 eV. The 2nd derivative spectra can be successfully fitted only by including two additional peaks in the energy region between 1 and 2 eV, as indicated by arrows in Fig. 2(c).

Figure 3 shows the dielectric function ($\varepsilon = \varepsilon_1 + i\varepsilon_2$) of the BFO thin film obtained from ellipsometric analysis. The overall spectral shape is very similar to those reported previously for bulk BFO and the BFO film.[22,23] The direct band gap energy E_g was estimated by extrapolating the linear fit using $(\alpha E)^2 \propto (E - E_g)$, where E is the photon energy and α is the absorption coefficient. Here, the absorption coefficient is derived from the relation $4\pi k/\lambda$, where λ is the photon wavelength and k is the imaginary part of the complex refractive index. The complex refractive index is converted from the relation $\sqrt{\varepsilon} = n + ik$. The magnitude of the band gap is about 2.73 eV at $T = 300$ K, which is similar to the values reported in the literature.[23–25] The prominent peaks in ε_2 at around 3.0 and 4.0 eV are assigned to charge transfer transitions from the valence band, consisting of the O 2*p* hybridized with Fe 3*d* and/or Bi 6*p* states, to the conduction bands composed of Fe 3*d* and Bi 6*p* states.[5,22,26]

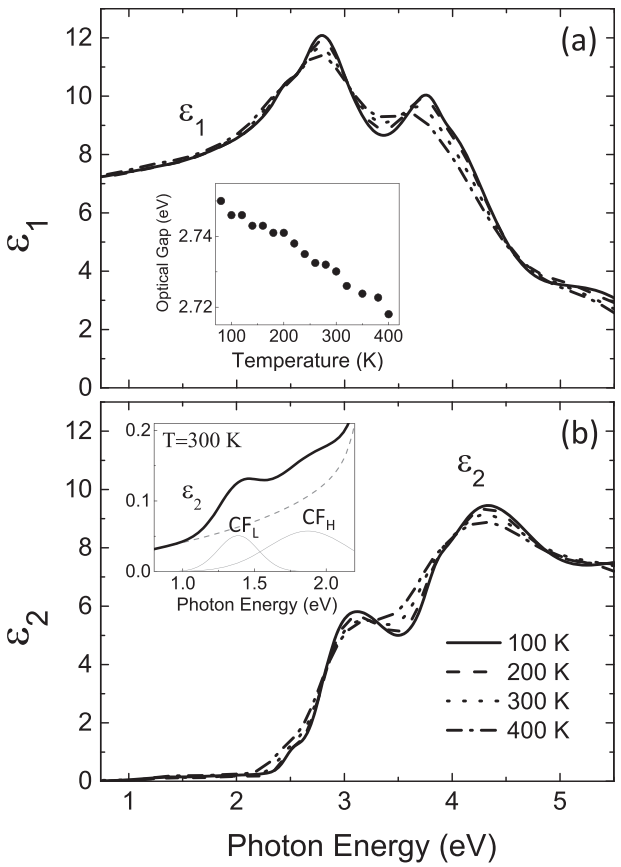

FIG. 3. (a) Real and (b) imaginary parts of dielectric functions at $T = 100$, 200, 300, and 400 K. The inset in (a) shows the magnitude of the optical gap as a function of T. The inset in (b) highlights the presence of two *d-d* crystal-field excitations, labeled as CF_L and CF_H. The dashed line represents the contribution from higher-energy optical transitions.

Two weak optical transitions can be identified below the optical band gap, as shown in the inset of Fig. 3(b). The peaks are centered at 1.38 and 1.87 eV at $T = 300$ K, which are close to those obtained from the optical absorption spectra of bulk BFO.[4,5] Their amplitudes were much smaller than those of the charge transfer transitions located at higher energies. The peak positions and weak strength of the two peaks are consistent with on-site Fe^{3+} CF transitions.[4–6] The two peaks may be attributed to $^6A_{1g} \rightarrow {}^4T_{1g}$ and $^6A_{1g} \rightarrow {}^4T_{2g}$ excitations, which are labeled as CF_L and CF_H, respectively. Observation of these *d-d* CF transitions from epitaxial BFO films as thin as ~70 nm demonstrates the excellent sensitivity of spectroscopic ellipsometry to the optical response of thin films.

Having identified the character of the optical transitions, we now discuss their evolution with T. We first focus on the *d-d* CF excitations, i.e., CF_L and CF_H. Figure 4 shows the T-dependent parameters (center energy, broadening parameter, and amplitude) obtained from fitting the dielectric function using Gaussian oscillators. We found that the center energies and broadening parameters show non-monotonic T dependence. In conventional semiconductors with electron-phonon interactions, the T dependences of the two parameters are known to follow the empirical Varshni equation or Bose-Einstein statistical factor, i.e., monotonic increase (decrease) in center energy (broadening parameters) followed by saturation at low T.[21,27] The center energies of both CF transitions show small changes with T. As T decreases to around 200 K, the center energies increase. At lower T, they decrease slightly. The lineshape broadening of the CF_L transition shows an anomaly, while that of CF_H decreases monotonically with decreasing T. The former has a minimum at T between 200 K and 300 K. A similar anomaly can be found in the amplitudes of both CF transitions, which exhibit a minimum at about 200 K. We note that the Raman experiments on BFO single crystals found a signature of spin reorientation transitions at 140 K and 200 K.[8] This suggests that the *d-d* CF transition anomaly in our BFO thin films may be linked to spin reorientation transitions.

With regard to the effect of spin reorientation on the amplitude of *d-d* transitions, the rotation of spins causes a distortion in the lattice structure through the magnetostrictive effect followed by a change in electronic state. Based on the interaction between lattice and electronic state, a decrease in Huang-Rhys electron-phonon coupling strength appears to occur below the spin reorientation temperature.[5]

It is worth noting that the oscillator strength of the CF_L transition in optical absorption spectra of BFO single crystals showed a minimum at about 150 K.[5] The contribution of the surface should be considered for thin films, and the spin reorientation effect in the region of the surface may be different from that in the bulk of the film media.[28] Differences in crystalline quality of single crystals and thin film may also make

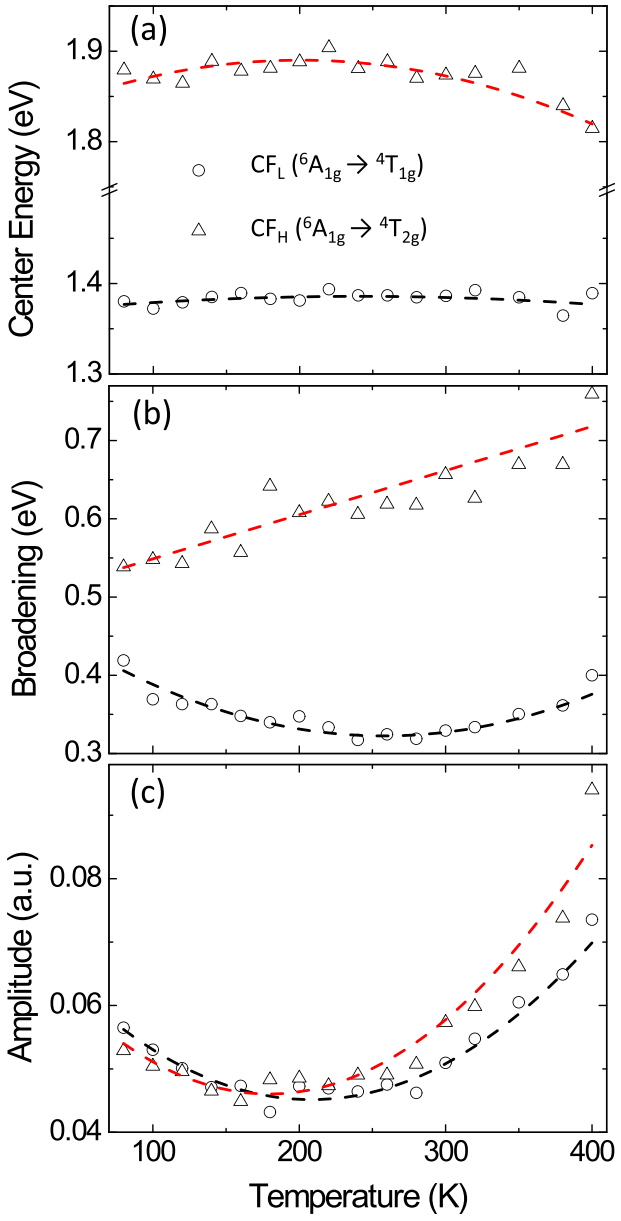

FIG. 4. Temperature-dependent parameters of Gaussian oscillators for the crystal field transitions (CF_L and CF_H). (a) Center energy. (b) Broadening parameter. (c) Amplitude.

a significant contribution. In the latter, strain from the substrate can affect the lattice structure. Such variations in lattice structure can cause a change in the spin states of Fe ions through the magnetoelastic effect. Therefore, spin reorientation seems to be affected by the strain, and vice versa, through a complementary process between the magnetoelastic and the magnetostrictive effects.

In addition, thin film is more susceptible to defect formation such as other crystalline and structural phases. The x-ray diffraction data from our BFO film shown in Fig. 1 support the absence of other Bi-Fe-O composite phases, such as $Bi_2Fe_4O_9$, which was reported to have an antiferromagnetic transition around 260 K.[29] However, possibility of the existence of other structural distortion either as small structural change or as small fraction with a slightly different symmetry cannot be excluded completely.[30]

We now discuss T dependence of charge transfer transitions located in the energy region between 2 and 5 eV. As shown in Fig. 3, the charge transfer transitions become narrower with decreasing T, which we attribute mainly to the electron-phonon interaction. With electron-phonon interactions, center energies of the charge transfer excitations increase, while broadening parameters decrease monotonically as T decreases.[21] As a result, the direct band gap increases linearly with decreasing T. The inset of Fig. 3(a) shows such a trend in T dependence of the band gap.

To obtain detailed information on the T dependence of the charge transfer transitions, we performed standard critical point (SCP) analysis of the 2nd derivatives of the dielectric functions ($d^2\varepsilon/dE^2$). SCP analysis is a conventional method to determine the critical point parameters such as energy threshold, broadening, amplitude, and phase angle of electronic transitions from the dielectric function.[21,31] The lineshape expressions are as follows:

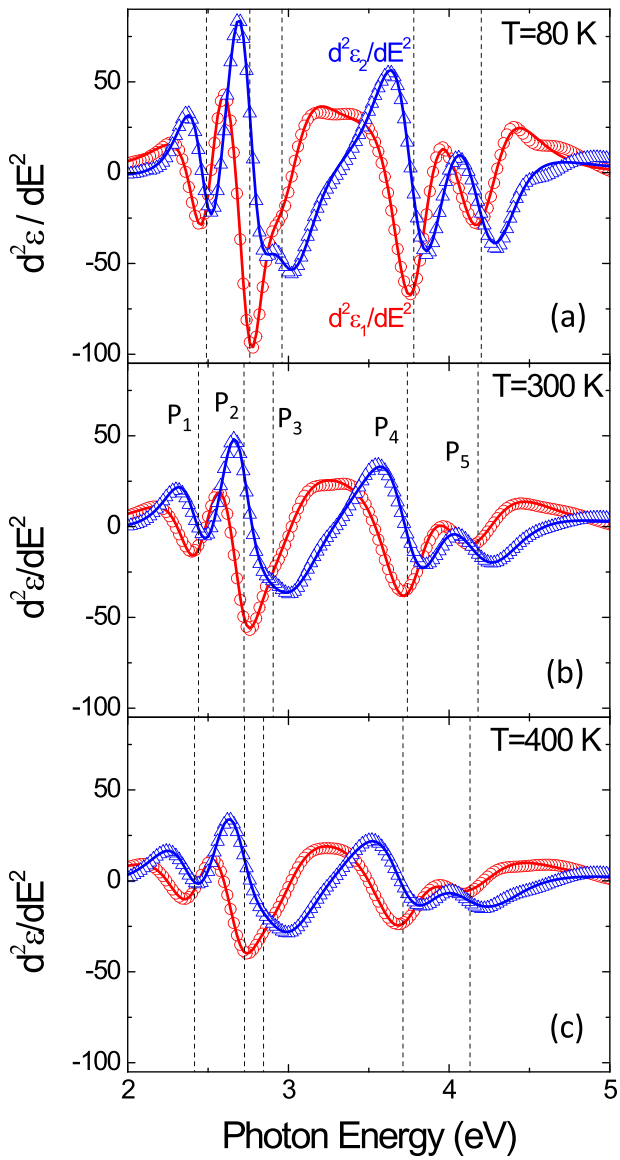

FIG. 5. The 2nd derivative of ε_1 (circles) and ε_2 (triangles) and their fits at (a) $T = 80$ K, (b) $T = 300$ K, and (c) $T = 400$ K using the SCP model. The vertical lines indicate threshold energy values of critical points (P_1, P_2, P_3, P_4, and P_5).

$$\frac{d^2\varepsilon}{dE^2} = \begin{cases} n(n-1)Ae^{i\phi}(E - E_{th} + i\Gamma)^{n-2}, & n \neq 0, \\ Ae^{i\phi}(E - E_{th} + i\Gamma)^{-2}, & n = 0, \end{cases} \quad (2)$$

where A is the amplitude, E_{th} is the threshold energy, Γ is the broadening parameter, and ϕ is the phase angle of the critical point. The exponent n has values of -1, $-1/2$, 0, $+1/2$ for excitonic, one-, two-, and three-dimensional lineshapes, respectively.

The 2nd derivative spectra reveal five peak structures labeled as P_i ($i = 1$, 2, 3, 4, and 5) in Fig. 5. The transition P_1 placed at around 2.5 eV is mostly attributed to the transition from the valence band to the oxygen vacancy level[32,33] or p-d transition $t_{1g}(\pi) \rightarrow t_{2g}$.[22] The transitions P_2, P_3, P_4, and P_5 are attributed to charge transfer transitions from O 2p mixed with Fe 3d to Fe 3d or to Bi 6p.[22,23,26] We note that by performing SCP analysis on the 2nd derivative spectra Choi *et al*. found four charge transfer transitions.[34] Whereas Choi *et al*. fitted the transition near 2.8 eV with a single oscillator; we found that transitions near 2.8 eV may be better described using two oscillators. Our result is consistent with that of Pisarev *et al*.[22] The splitting of the transition near 2.8 eV into two peaks, P_2 and P_3, may be attributed to a trigonal distortion of the FeO_6 octahedra.[22]

Figure 6 shows T-dependent values of threshold energy, broadening parameter, amplitude, and phase angle obtained from fitting the 2nd derivative spectra using Eq. (2). The best fit was obtained with an excitonic lineshape ($n = -1$) for all critical points. For an excitonic lineshape, the phase angle ϕ can be interpreted as a coupling parameter between the discrete excitation and an overlapping continuous background due to interband transitions.[21] In an optical study of BFO single crystals, the best fit was obtained with $n = -1$ for the lowest-energy peak and $n = 0$ for the other three peaks.[34] We speculate that such low dimensionalities ($n = -1$) of the critical points may be due to high defect density in the BFO film.

The threshold energies of the charge transfer transitions show gradual decrease with increasing T, as shown in Fig. 6(a). This can be described by electron-phonon interactions.[21] A closer inspection of the threshold energies reveals an interesting trend in the evolution of the transitions P_2 and P_3 located in the energy region between 2.8 and 3.0 eV. This two-peak structure may result from trigonal distortion of the FeO_6 octahedra.[22] As T increases the energy separation between the two transitions becomes noticeably smaller. This may indicate a weakening of the trigonal distortion at high T.

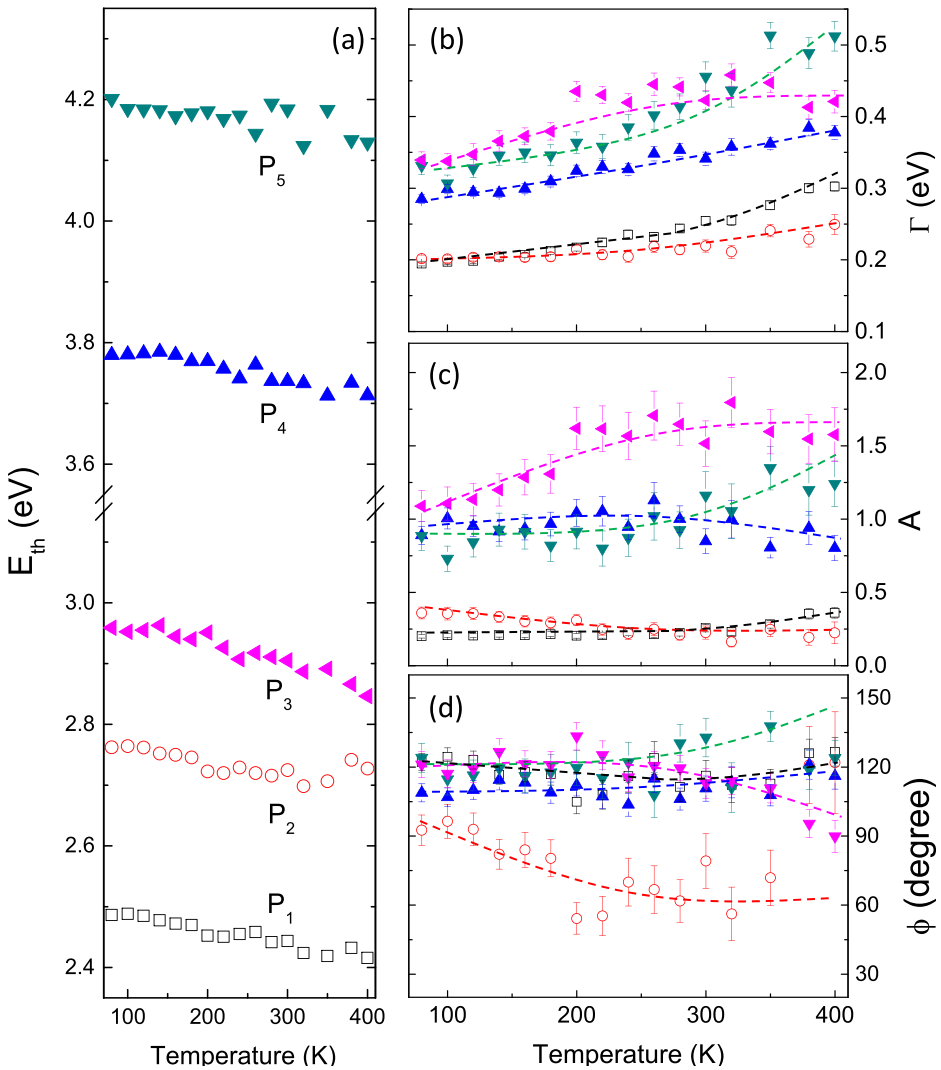

FIG. 6. Temperature dependence of (a) threshold energy, (b) broadening parameter, (c) amplitude, and (d) excitonic phase angle of the charge transfer transitions obtained from the SCP analysis of the 2nd derivatives of dielectric functions.

The T dependence of the broadening parameters of the transitions P_1, P_2, P_4, and P_5 displayed in Fig. 6(b) seems to follow the empirical Varshni equation.[21] The behavior of the broadening parameter of the transition P_3 differs from the others, i.e., it decreases only below 200 K and no saturation signature is observed. We note that at 200 K the *d-d* CF transitions in the optical data also exhibit an anomaly, and Raman studies showed an indication of spin-reorientation transition. Further studies are needed to find the relevance of spin reorientation to this unusual behavior in the broadening parameter of the transition P_2.

IV. CONCLUSION

We investigated the temperature dependence of electronic transitions of rhombohedral $BiFeO_3$ film grown on $SrTiO_3$ (001) substrate using spectroscopic ellipsometry. We observed two *d-d* crystal field transitions in the energy region between 1 and 2 eV. The *d-d* crystal field transitions showed an abnormal temperature dependence that cannot be explained in terms of electron-phonon interactions. We discussed the relevance of the abnormal temperature dependence of the *d-d* crystal field to a spin reorientation transition. By standard critical point model analysis of the charge transfer transitions, we identified five charge transfer transitions and obtained detailed information on the temperature dependence of their critical point parameters.

ACKNOWLEDGMENTS

This work was supported by the Institute for Basic Science (IBS) in Korea (IBS-R009-D1) and by the Basic Science Research Program through the National Research Foundation of Korea funded by the Ministry of Science, ICT & Future Planning (2012R1A1A1013274).

[1]G. A. Smolenskii, V. Isupov, A. Agranovskaya, and N. Kranik, Sov. Phys. Solid State **2**, 2651 (1961).
[2]P. Fischer, M. Polomska, I. Sosnowska, and M. Szymanski, J. Phys. C **13**, 1931 (1980).
[3]W. Eerenstein, N. D. Mathur, and J. F. Scott, Nature **442**, 759 (2006).
[4]M. O. Ramirez, A. Kumar, S. A. Denev, N. J. Podraza, X. S. Xu, R. C. Rai, Y. H. Chu, J. Seidel, L. W. Martin, S.-Y. Yang, E. Saiz, J. F. Ihlefeld, S. Lee, J. Klug, S. W. Cheong, M. J. Bedzyk, O. Auciello, D. G. Schlom, R. Ramesh, J. Orenstein, J. L. Musfeldt, and V. Gopalan, Phys. Rev. B **79**, 224106 (2009).
[5]X. S. Xu, T. V. Brinzari, S. Lee, Y. H. Chu, L. W. Martin, A. Kumar, S. McGill, R. C. Rai, R. Ramesh, V. Gopalan, S. W. Cheong, and J. L. Musfeldt, Phys. Rev. B **79**, 134425 (2009).
[6]B. Ramachandran, A. Dixit, R. Naik, G. Lawes, and M. S. Ramachandra Rao, Phys. Rev. B **82**, 012102 (2010).
[7]M. Cazayous, Y. Gallais, and A. Sacuto, Phys. Rev. Lett. **101**, 037601 (2008).
[8]M. K. Singh, R. S. Katiyar, and J. F. Scott, J. Phys.: Condens. Matter **20**, 252203 (2008).
[9]N. Koshizuka and S. Ushioda, Phys. Rev. B **22**, 5394 (1980).
[10]K. P. Belov, A. K. Zvezdin, A. M. Kadomtseva, and R. Z. Levitin, Usp. Fiz. Nauk **119**, 447 (1976).
[11]V. Železný, D. Chvostová, L. Pajasová, I. Vrejoiu, and M. Alexe, Appl. Phys. A **100**, 1217 (2010).
[12]K. Jiang, J. J. Zhu, J. D. Wu, J. Sun, Z. G. Hu, and J. H. Chu, ACS Appl. Mater. Interfaces **3**, 4844 (2011).
[13]P. Rovillain, M. Cazayous, Y. Gallais, and A. Sacuto, Phys. Rev. B **79**, 180411 (2009).
[14]J. F. Scott, M. K. Singh, and R. S. Katiyar, J. Phys.: Condens. Matter **20**, 322203 (2008).
[15]S. A. T. Redfern, C. Wang, J. W. Hong, G. Catalan, and J. F. Scott, J. Phys.: Condens. Matter **20**, 425205 (2008).
[16]H. Fujiwara, *Spectroscopic Ellipsometry: Principles and Applications* (Wiley, Chichester, England, 2007).
[17]S. S. A. Seo, M. J. Han, G. W. J. Hassink, W. S. Choi, S. J. Moon, J. S. Kim, T. Susaki, Y. S. Lee, J. Yu, C. Bernhard, H. Y. Hwang, G. Rijnders, D. H. A. Blank, B. Keimer, and T. W. Noh, Phys. Rev. Lett. **104**, 036401 (2010).
[18]S. K. Singh, Y. K. Kim, H. Funakubo, and H. Ishiwara, Appl. Phys. Lett. **88**, 162904 (2006).
[19]D. E. Aspnes and A. A. Studna, Phys. Rev. B **27**, 985 (1983).
[20]J. A. Woollam, *Guide to Using WVASE32* (J.A. Woollam Co., Inc., 2002).
[21]P. Lautenschlager, M. Garriga, S. Logothetidis, and M. Cardona, Phys. Rev. B **35**, 9174 (1987).
[22]R. V. Pisarev, A. S. Moskvin, A. M. Kalashnikova, and T. Rasing, Phys. Rev. B **79**, 235128 (2009).
[23]P. Chen, N. J. Podraza, X. S. Xu, A. Melville, E. Vlahos, V. Gopalan, R. Ramesh, D. G. Schlom, and J. L. Musfeldt, Appl. Phys. Lett. **96**, 131907 (2010).
[24]S. R. Basu, L. W. Martin, Y. H. Chu, M. Gajek, R. Ramesh, R. C. Rai, X. Xu, and J. L. Musfeldt, Appl. Phys. Lett. **92**, 091905 (2008).
[25]A. Kumar, R. C. Rai, N. J. Podraza, S. Denev, M. Ramirez, Y.-H. Chu, L. W. Martin, J. Ihlefeld, T. Heeg, J. Schubert, D. G. Schlom, J. Orenstein, R. Ramesh, R. W. Collins, J. L. Musfeldt, and V. Gopalan, Appl. Phys. Lett. **92**, 121915 (2008).
[26]H. Wang, Y. Zheng, M.-Q. Cai, H. Huang, and H. L. W. Chan, Solid State Commun. **149**, 641 (2009).
[27]S. Zollner, M. Garriga, J. Kircher, J. Humlíček, M. Cardona, and G. Neuhold, Phys. Rev. B **48**, 7915 (1993).
[28]T. Herrmann, M. Potthoff, and W. Nolting, Phys. Rev. B **58**, 831 (1998).
[29]A. K. Singh, S. D. Kaushik, B. Kumar, P. K. Mishra, A. Venimadhav, V. Siruguri, and S. Patnaik, Appl. Phys. Lett. **92**, 132910 (2008).
[30]C. Himcinschi, A. Bhatnagar, A. Talkenberger, M. Barchuk, D. R. T. Zahn, D. Rafaja, J. Kortus, and M. Alexe, App. Phys. Lett. **106**, 012908 (2015).
[31]H. Lee, Y. S. Kang, S.-J. Cho, B. Xiao, H. Morkoç, and T. D. Kang, Appl. Phys. Lett. **86**, 262902 (2005).
[32]S. Ju and T.-Y. Cai, Appl. Phys. Lett. **95**, 231906 (2009).
[33]S. J. Clark and J. Robertson, Appl. Phys. Lett. **94**, 022902 (2009).
[34]S. G. Choi, H. T. Yi, S.-W. Cheong, J. N. Hilfiker, R. France, and A. G. Norman, Phys. Rev. B **83**, 100101 (2011).